

NRL FR-8765

Mirror Antenna Dual-Band Lightweight Mirror
Design

Dean D. Howard
David C. Cross

December 12, 1983

Naval Research Laboratory
Washington D.C.

REPORT DOCUMENTATION PAGE		READ INSTRUCTIONS BEFORE COMPLETING FORM
1. REPORT NUMBER NRL Report 8765	2. GOVT ACCESSION NO.	3. RECIPIENT'S CATALOG NUMBER
4. TITLE (and Subtitle) MIRROR ANTENNA DUAL-BAND LIGHTWEIGHT MIRROR DESIGN	5. TYPE OF REPORT & PERIOD COVERED Interim report - October 1979 - July 1983	
	6. PERFORMING ORG. REPORT NUMBER	
7. AUTHOR(s) Dean D. Howard and David C. Cross	8. CONTRACT OR GRANT NUMBER(s)	
9. PERFORMING ORGANIZATION NAME AND ADDRESS Naval Research Laboratory Washington, DC 20375	10. PROGRAM ELEMENT, PROJECT, TASK AREA & WORK UNIT NUMBERS 62712N; SF12-131-691; 53-0616-03	
11. CONTROLLING OFFICE NAME AND ADDRESS Naval Sea Systems Command, Washington, DC 20360 Naval Material Command, Washington, DC 20360	12. REPORT DATE December 12, 1983	
	13. NUMBER OF PAGES 25	
14. MONITORING AGENCY NAME & ADDRESS (if different from Controlling Office)	15. SECURITY CLASS. (of this report) UNCLASSIFIED	
	15a. DECLASSIFICATION/DOWNGRADING SCHEDULE	
16. DISTRIBUTION STATEMENT (of this Report) Approved for public release; distribution unlimited.		
17. DISTRIBUTION STATEMENT (of the abstract entered in Block 20, if different from Report)		
18. SUPPLEMENTARY NOTES		
19. KEY WORDS (Continue on reverse side if necessary and identify by block number) Radar Track-while-scan Mirror scan radar Weapon control Mirror tracker radar Fire control Anti-air warfare Point defense		
20. ABSTRACT (Continue on reverse side if necessary and identify by block number) The design of a dual-band half-wave-plate mirror for a two-axis beam scan mirror antenna is described. The solution for design parameters is given for perfect 90° polarization rotation at a given aspect angle for each of the two bands. The process for optimizing the design for the full desired range of aspect angle is described. Practical fabrication considerations are discussed along with inclusion of capacitive susceptance of a protective covering in the design theory. Calculated performance is compared with measurements of mirror samples.		

CONTENTS

INTRODUCTION	1
BACKGROUND	2
SINGLE-GRID HALF-WAVE-PLATE DESIGN	4
DUAL-GRID DUAL-BAND HALF-WAVE-PLATE DESIGN	6
DESIGN OPTIMIZATION FOR DUAL-BAND TWO-AXIS MIRROR ANTENNA	8
SPECIFIC PRACTICAL DESIGN TASKS	14
TWIST REFLECTOR FINAL DESIGN	15
MIRROR FABRICATION	17
SUMMARY	20
ACKNOWLEDGMENTS	20
REFERENCES	20
APPENDIX – PERFORMANCE VS PLANE OF ANGLE OF INCIDENCE	21

MIRROR ANTENNA DUAL-BAND LIGHTWEIGHT MIRROR DESIGN

INTRODUCTION

Several types of microwave antennas use a half-wave plate or polarization rotation mirror sometimes called a polarization twist reflector or simply a twist reflector. Some configurations called mirror scan antennas use a rotatable flat mirror as a convenient means for moving the antenna beam. The polarization rotation is used, as described below, to see through antenna surfaces which would otherwise cause radio-frequency (rf) energy blockage.

One version of the mirror antenna uses two-axis tilting of the mirror as a convenient means for beam movement in two-angle coordinates. Figure 1 is a simplified view of one scan axis. A fixed feed and radome-supported paraboloid collimate the radar beam. The beam then propagates toward a mirror which may be tilted by an angle θ to obtain a 2θ displacement of the radiated beam. This factor of two permits very wide-angle coverage with a compact structure and is advantageous for accomplishing high-acceleration beam movement.

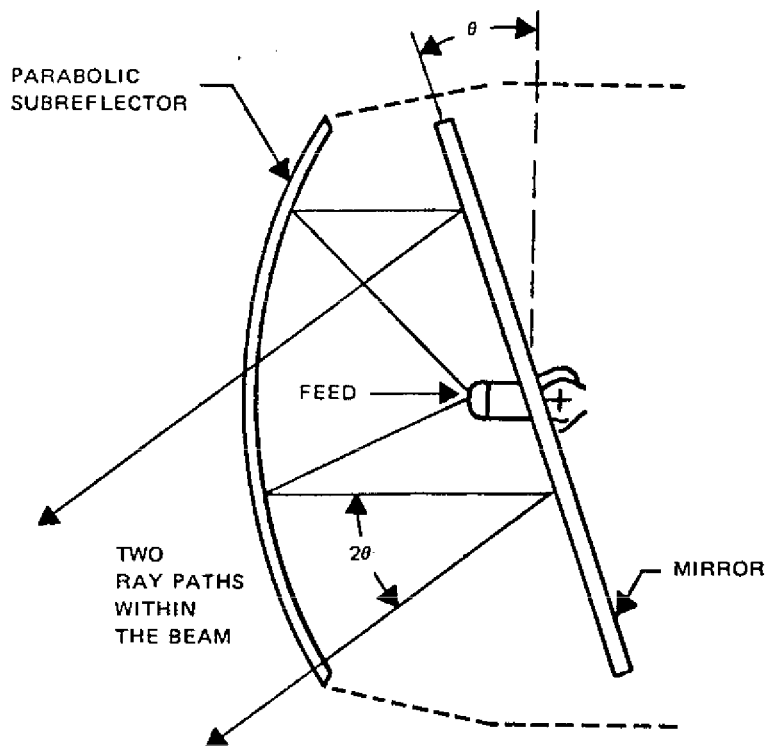


Fig. 1 — Basic two-axis mirror antenna technique

The paraboloid is a grid of conductors parallel to the feed polarization and looks like a solid reflector to the radiation from the feed. The mirror is a half-wave plate or polarization twist reflector which rotates the polarization 90° and makes the grid paraboloid transparent to the reflected radiated

energy. The received energy from target echoes, in a radar application, has its polarization rotated (by the mirror) back to an orientation parallel to the paraboloid grid so that it is focused on the feed.

The mirror may be gimbaled for two axes of tilt, as illustrated in Fig. 2, to perform a two-angle coordinate scan with greater than half-hemisphere coverage. Major advantages of the mirror scan antenna include (a) the capacity for beam scanning with no waveguide rotary joints for reliability and low-loss operation, (b) the very wide-angle scan capability with low-scan loss, and (c) the ability of beam scanning with high acceleration and velocity because the only moving parts are the lightweight mirror and its actuators.

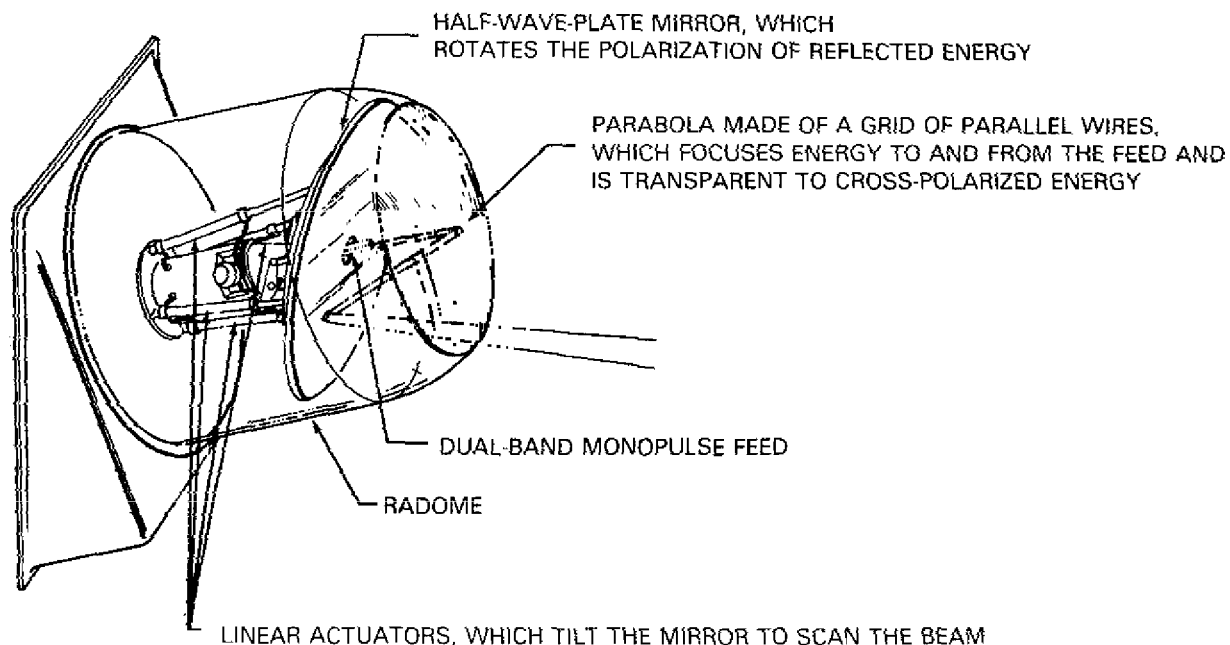


Fig. 2 — Two-axis mirror antenna with linear actuators

Mirror scan antennas in present use include an Israeli airborne radar application [1] patterned after an experimental Westinghouse monopulse radar wide-angle scan mirror antenna (Westinghouse Model WX-200). The current systems are for single-band operation; however another major advantage of the mirror scan antenna is its potential for dual-band or multiband operation. The major design problem is the dual-band mirror.

This report covers the theory, basic design, optimization, and fabrication of a lightweight dual-band mirror for the mirror-scan antenna. The background section discusses the basic half-wave-plate design and the current approaches for wide-band operation. This background section provides the basis for the design described here and its dual-band optimization for a wide range of aspect angles.

BACKGROUND

Figure 3 represents a simple single-grid mirror. The illuminating rf energy first arrives at a grid of wires oriented at 45° to its polarization. This grid divides the energy into two components, one parallel to the grid which is reflected by the grid and the other perpendicular to the grid which passes through the grid and is reflected by the solid conducting surface behind the grid.

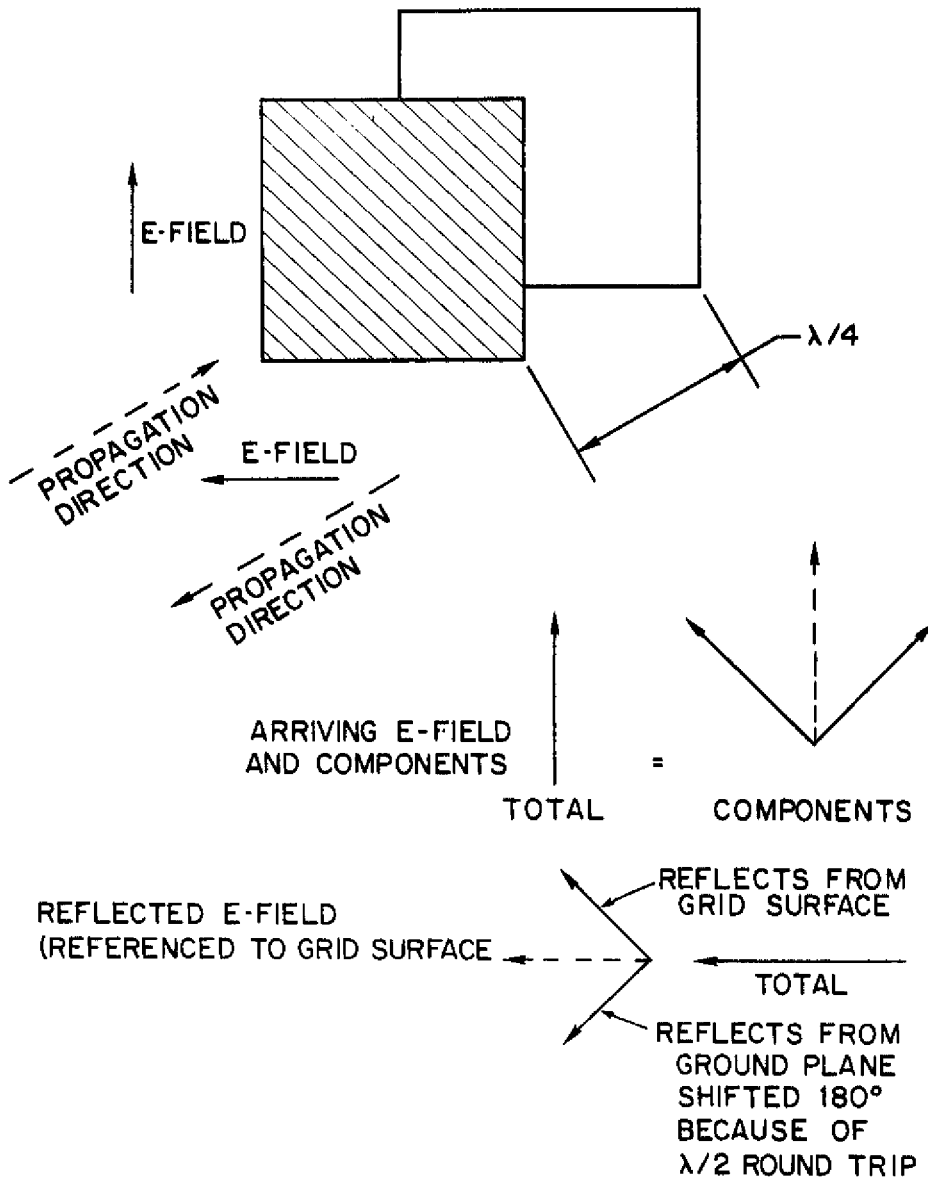


Fig. 3 — Basic half-wave-plate (twist reflector) design

The simplest version of the half-wave plate assumes a dense grid spaced a quarterwave above the conducting surface. The dense grid looks like a solid conductor surface to the parallel polarization component which reflects at that point. The perpendicular component travels the additional distance to the conducting surface and back for a half-wave additional two-way path when it arrives back at the grid. The perpendicular polarization component is therefore delayed 180° relative to the parallel component when it arrives back at the grid as illustrated in Fig. 3. The resultant sum of the components is a polarization vector at 90° to the arriving polarization; thus, the desired 90° rotation of the polarization is accomplished.

A more general analysis by Hannan [2] assumes a variable normalized grid susceptance B_w and variable spacing between the grid and the conducting surface. Because of a lower density grid, some of the parallel polarization component can pass through the grid. These two parts of the parallel com-

ponent can then be combined to produce the desired phase relation with the perpendicular component for a given relation between B_w and distance L between the grid and conducting plane. Hannan shows that the least frequency and aspect sensitivity occurs for a normalized grid susceptance of -2.05 and a grid spacing of 0.358λ from the conducting surface. The theory leading to these results will be covered under Single-Grid Half-Wave-Plate Design.

An ultrawide-band mirror technique invented by Lewis and Shelton [3] is based on a different mirror configuration which allows a controlled movement of effective reflection points as a function of frequency for each of the two polarization components. This control provides the means for maintaining a quarter-wavelength spacing essentially independent of frequency.

The ultrawide-band performance is accomplished with orthogonal interlaced arrays of log-periodic elements, each set coupling to one of the orthogonal polarization components. By proper design, the effective reflection point within the elements will move as a function of frequency to provide the desired relative phase between orthogonal components.

The ultrawide-band design is excellent for applications such as the mirror scan antenna configuration [3] invented by Lewis [4] where the mirror rotates continuously at constant velocity, and mass is not a problem. Lightweight versions may be possible, but, it is expected that the thinnest and lightest-weight mirror for two-frequency operation is a two-grid design as described in this report.

An example of a two-grid mirror designed for two frequencies for the purpose of providing a moderately wide-band twist reflector is given by Josefsson [5] who shows that a mirror with two parallel grids can be designed for theoretically perfect 90° polarization rotation at each of two frequencies for a given relation of grid susceptances and spacing. Also, for a reasonable separation of the two design frequencies, good performance is obtained in the band between the two frequencies. Josefsson describes a specific example of susceptance values and selection of a ratio of the two design frequencies of 1.5 to demonstrate the wide-band capability. His analysis is limited to only the normal aspect of the mirror. He further indicates that theoretical coverage of both wide bandwidth and variable aspect angle "will certainly be very complicated." Although the theory becomes complex for optimizing over variable aspect, experimentation with parameters, as described below, leads to good optimization over the desired aspect range. The work of Hannan and Josefsson provides a useful aid in the design of the dual-band mirror with operation over a wide aspect range.

SINGLE-GRID HALF-WAVE-PLATE DESIGN

The single-grid, single-band mirror design by Hannan is a useful basis for polarization twist mirror designs. His work covers the basic transmission line analysis with consideration of the effect of a range of aspect angles. He also discusses practical considerations in mirror construction including theoretical treatment of the effect of a dielectric layer for support of the grid and dielectric core.

Hannan's theoretical analysis is based on the mirror geometry as illustrated in Fig. 4(a) and the equivalent transmission lines, Fig. 4(b), for perpendicular and parallel polarization where λ is wavelength and α is aspect angle ($\alpha = 0$ is the normal to the mirror as assumed in the above discussions). Figure 4(b) also indicates that for an inductive grid, the apparent short circuit or reflection point is behind the grid (between the grid and conducting surface).

An approximation to the normalized susceptance of the wire grid is

$$\frac{B_w}{Y_0} \approx -\frac{\lambda}{S \cos \alpha} \cdot \frac{1}{\ln \left[\frac{S}{\pi D} \right]} \quad (1)$$

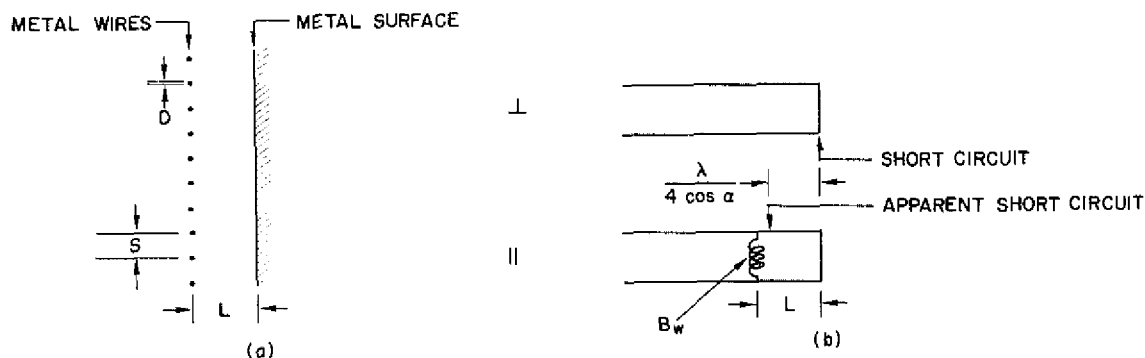


Fig. 4 — General design with wires; (a) cross section, and (b) equivalent transmission lines

which is a good approximation when the wire spacing S is small compared to a wavelength and the wire diameter D is much smaller than S .

To obtain the desired 90° polarization twist, the admittance Y_{\perp} of the transmission line for the perpendicular polarization component must equal the reciprocal of the admittance of the parallel component Y_{\parallel} or

$$Y_{\perp} = \frac{1}{Y_{\parallel}} \quad (2)$$

The normalized admittance values observed at the location of the grid are

$$\frac{Y_{\perp}}{Y_0} = -j \cot \left(\frac{2\pi L \cos \alpha}{\lambda} \right) \quad (3)$$

$$\frac{Y_{\parallel}}{Y_0} = -j \cot \frac{2\pi L \cos \alpha}{\lambda} + j \frac{B_w}{Y_0} \quad (4)$$

where Y_0 is the susceptance of free space.

The value of B_w for 90° polarization twist is obtained by substituting Eqs. (3) and (4) in Eq. (2) giving

$$\frac{B_w}{Y_0} = 2 \csc \left(\frac{4\pi L \cos \alpha}{\lambda} \right) \quad (5)$$

Observe that the normalized susceptance B_w/Y_0 can have any value from infinity to two and, for negative susceptance of a grid of wires, the spacing between the grid and conducting surface must be between $\lambda/4$ and $\lambda/2$.

From a practical construction consideration, the smallest value of B_w/Y_0 (corresponding to $L = 0.375\lambda$ and $\alpha = 0$) is desirable because a minimum number of conductors are required for a given wire size. Also, by analyzing for minimum sensitivity to frequency and aspect angle, Hannan solves for specific optimum values and obtains

$$\frac{L \cos \alpha}{\lambda} = 0.358 \quad \text{and} \quad B_w/Y_0 = -2.05.$$

These values are fortunately close to the desired minimum value.

Hannan further considers the effect of a dielectric core between the grid and conducting surface and the effect of the capacitive susceptance of a dielectric skin for covering and supporting the grid structure. In general, a low-loss, low-dielectric constant core and a thin (in wavelength) low-loss dielectric skin can be used with little effect on performance. The dielectric constant of the core is considered in calculating electrical distance between the grid and conducting surface. The thin dielectric skin provides a capacitive (positive) susceptance which is compensated by a smaller grid-to-conducting-surface spacing.

DUAL-GRID DUAL-BAND HALF-WAVE-PLATE DESIGN

The analysis for the dual-grid design is similar to that by Hannan for the single grid. The dual-grid configuration is described in Fig. 5(a). Using the symbols of Fig. 5(a), the susceptances for Grid No. 1 are

$$\frac{B_{w1}}{Y_0} = - \frac{\lambda}{S_1 \cos \alpha} \cdot \frac{1}{\ln \left[\frac{S_1}{\pi d_1} \right]} \tag{6}$$

and Grid No. 2 are

$$\frac{B_{w2}}{Y_0} = - \frac{\lambda}{S_2 \cos \alpha} \cdot \frac{1}{\ln \left[\frac{S_2}{\pi d_2} \right]} \tag{7}$$

Also, the susceptance for the dielectric skin is

$$\frac{B_{s1}}{Y_0} = \frac{2\pi T(\epsilon_s - 1)}{\lambda} \tag{8}$$

where T is the skin thickness ($T \ll \lambda$) and ϵ_s is the skin dielectric constant.

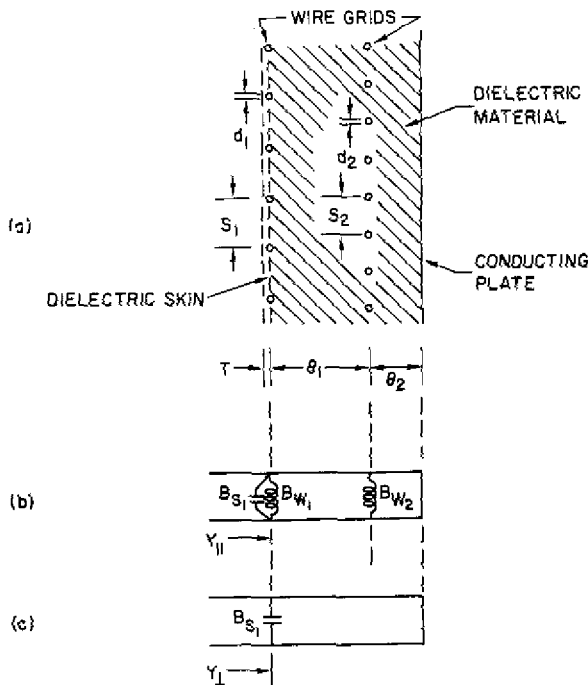


Fig. 5 — Two-grid mirror design; (a) cross section, (b) equivalent transmission line for the parallel polarization component, and (c) equivalent transmission line for the perpendicular polarization component

The skin susceptance equation is valid only at normal incidence; however, as indicated by Hannan, it yields approximately the best average value for *E*-plane and *H*-plane oblique incidence.

The values of θ_1 and θ_2 are the electrical distances indicated including the effect of the supporting dielectric core.

The mirror is to be designed for operation at two frequencies f_a and f_b . The frequency f_a is greater than f_b by a ratio R . All values for B 's and θ 's are proportional or inversely proportional to the frequency. For convenience, all values of B 's and θ 's are calculated for f_b and values for f_a will be the B 's and θ 's calculated for f_b and modified by R .

The equivalent transmission lines for the parallel and perpendicular polarization components are given in Figs. 5(b) and 5(c) where the grid locations are indicated by their susceptance symbols. The line admittances are calculated at the location of the outer grid (Grid No. 1) by moving admittances from the shorted end to the position of Grid No. 1 and using the usual equation

$$\frac{Y_c}{Y_0} = \frac{\frac{Y_d}{Y_0} + j \tan \theta}{1 + j \left[\frac{Y_d}{Y_0} \tan \theta \right]} \quad (9)$$

where Y_c is the normalized admittance observed at point C resulting from an admittance Y_d at point d where their separation is an electrical length θ .

In the simpler case of Fig. 5(c), for perpendicular polarization, the admittance of the short is moved through a distance $\theta_1 + \theta_2$ (bypassing Grid No. 2 which is invisible to parallel polarization) and added to the admittance of the dielectric skin B_s giving (at f_b)

$$\frac{Y_{bl}}{Y_0} = j B_s - j \cot (\theta_1 + \theta_2) \quad (10)$$

The process for parallel polarization with the transmission line of Fig. 5(b) is similar. The admittance of the short is moved through distance θ_2 to Grid No. 2 and added to the admittance of Grid No. 2. This combined admittance is then moved through distance θ_1 to Grid No. 1. It is then added to the admittance of both Grid No. 1 and the dielectric skin giving (at f_b)

$$\frac{Y_{b||}}{Y_0} = j B_s + j B_1 + \frac{j(B_2 - \cot \theta_2) + j \tan \theta_1}{1 - (B_2 - \cot \theta_2) \tan \theta_1} \quad (11)$$

For 90° polarization twist, the admittance of the two lines must be reciprocals as stated in Eq. (1). By substitution, the relation between parameters is (at f_b)

$$B_1 = \frac{1}{\cot (\theta_1 + \theta_2) - B_s} - B_s - \frac{B_2 - \cot \theta_2 + \tan \theta_1}{1 - B_2 \tan \theta_1 + \cot \theta_2 \tan \theta_1} \quad (12)$$

The same analysis is performed at frequency f_a by using the ratio R as previously described to scale susceptance and distance for frequency f_b . The resulting line susceptances are (at f_a)

$$Y_{al} = j R B_s - j \cot (R\theta_1 + R\theta_2) \quad (13)$$

and (at f_a)

$$Y_{a||} = j R B_s + j \frac{B_1}{R} + \frac{j \frac{B_2}{R} - \cot R\theta_2 + j \tan R\theta_1}{1 - \frac{B_2}{R} - \cot R\theta_2 \tan R\theta_1} \quad (14)$$

The modification of Eqs. (10) and (11) by R corresponds to the relations that the capacitive susceptance is proportional to f , the inductive susceptance of the grids are inversely proportional to f , and the electrical length of a given distance is proportional to f . By equating reciprocals of admittances, the following relation between parameters is determined (at f_a):

$$B_1 = \frac{R}{RB_s \cdot \cot R(\theta_1 + \theta_2)} - \frac{B_2 - R \cot(R\theta_2) + R \tan(R\theta_1)}{1 - \frac{B_2}{R} \tan(R\theta_2) + \cot(R\theta_2) \tan(R\theta_1)} \quad (15)$$

Equations (12) and (15) each allow choice of values for B_s , B_2 , θ_1 , and θ_2 . To satisfy the reciprocal relation of Y_{\perp} and Y_{\parallel} for $f_{(a)}$ and $f_{(b)}$ simultaneously, these equations may be equated to each other resulting in a quadratic relation for B_2 in terms of B_s , θ_1 , and θ_2 :

$$B_2^2 [V - Y(1 + SV)] + B_2 [W + VX - Z(1 + SV) - Y(SW + T)] + WX - Z(SV + T) = 0 \quad (16)$$

where

$$S = R \tan R(\theta_1 + \theta_2) - \tan(\theta_1 + \theta_2),$$

$$T = \tan \theta_1 - \cot \theta_2,$$

$$V = \tan \theta_1,$$

$$W = 1 + \cot \theta_2 \tan \theta_1,$$

$$X = R [\tan(R\theta_1) - \cot(R\theta_2)],$$

$$Y = -\frac{\tan}{R}(R\theta_1), \text{ and}$$

$$Z = 1 + \cot(R\theta_2) \tan(R\theta_1).$$

In addition, the effect of aspect angle α must also be taken into account in the values of grid susceptances (B_1 and B_2) and electrical lengths (θ_1 and θ_2). Observe from Eq. (1) that grid susceptance is approximately inversely proportional to $\cos \alpha$. Also, the electrical lengths of θ_1 and θ_2 are proportional to $\cos \alpha$ (see Ref. 3). Therefore, θ_1 and θ_2 can be replaced by $\theta_1 \cos \alpha$ and $\theta_2 \cos \alpha$ respectively. Using Eq. (1) for grid susceptances and the above substitutions for θ_1 and θ_2 provides the aspect angle relation when calculating Y_{\perp} and Y_{\parallel} .

The equations allow the selection of parameters for the desired 90° polarization twist at each of two frequencies for a given aspect angle. Consequently, the performance will be in error to some degree at all other aspect angles. The following is a discussion of the procedure used to optimize performance for the mirror antenna application.

DESIGN OPTIMIZATION FOR DUAL-BAND TWO-AXIS MIRROR ANTENNA

To design the dual-band polarization twist mirror for operation over a range of aspect angles, it is necessary to provide a measure of performance at aspect angles other than the aspect of perfect 90° polarization twist, and to investigate how the parameters may be optimized for best overall performance. One way of examining the performance of the mirror at other aspect angles is to calculate the amount of undesired polarization energy. The attenuation of undesired polarization P_u given by Ref. 5 is

$$P_u = 1 + \left[\frac{Y_{\parallel} - Y_{\perp}}{1 + Y_{\parallel} Y_{\perp}} \right]^2 \quad (17)$$

where Y_{\perp} and Y_{\parallel} and pure susceptance.

The performance is evaluated by plotting P_u of Eq. (17) vs aspect angle. The smaller the value of $P(u)$ the better the performance.

Aspect angle has generally been assumed, in most references, to be in a plane perpendicular to the grid wires such as the angle α illustrated in Fig. 6. This assumption is of some concern, since it is not obvious that grid susceptances will have the same function vs aspect angle for aspect angles in other planes. An example is angle β in Fig. 6 in a plane parallel to the grid wires.

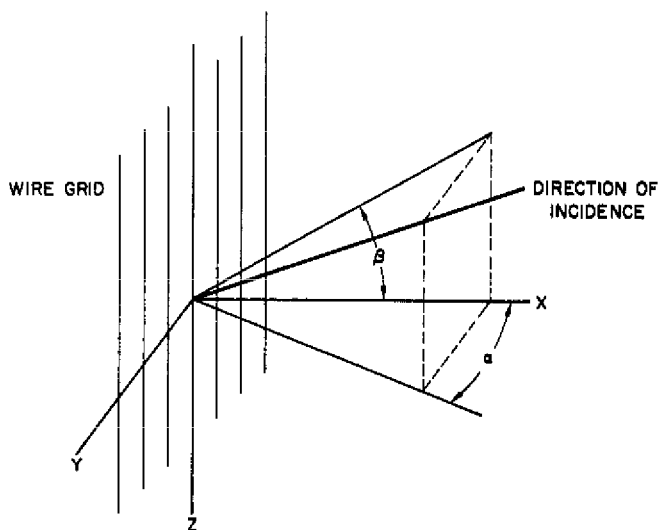


Fig. 6 — Planar wire grid with a plane wave at arbitrary incidence

Wait [6] analyzed the performance for arbitrary incidence angles and gave a more generalized form for grid susceptance

$$\frac{B_w}{Y_0} = \frac{\lambda}{S \cos \alpha \cos \beta} \cdot \frac{1}{\ln \left(\frac{S}{\pi d} \right)} \quad (18)$$

where α and β are defined in Fig. 6,
 S is grid wire separation (between centers), and
 d is grid wire diameter.

One problem is that operational angles of incidence will include aspect angles in planes at 45° to the wire grid which are not a simple relation to α and β . This problem is discussed in the appendix of this report, showing that aspect angle α in a 45° plane gives the relation

$$\frac{B_w(45)}{Y_0} = \frac{\lambda}{S \left[\frac{1 + (\cos \gamma)^2}{2(\cos \gamma)^2} \right]} \cdot \frac{1}{\ln \left(\frac{S}{\pi d} \right)} \quad (19)$$

Although this function appears significantly different from Eq. (18), the difference is small over the range of aspect angles of interest. Also, as described in the appendix, the resultant performance plots, which are discussed below, have insignificant differences between the parallel or perpendicular aspect planes and the 45° aspect plane. Therefore, performance is discussed below on the basis of aspect

angle α where it is assumed that performance for aspect angles in other planes will be the same or have insignificant differences.

Equation (17) was programmed to plot P_u vs aspect angle. Figure 7 is a typical plot with the mirror parameters chosen to give good overall performance. The parameters are determined for a given aspect angle. As seen in the plot, infinite attenuation of the undesired polarization component is achieved at that aspect angle. The lower frequency performance holds its shape consistently for a wide range of parameters. The higher frequency is observed to have a second performance peak at a wider aspect angle, which is useful for providing good operation over a wider aspect range.

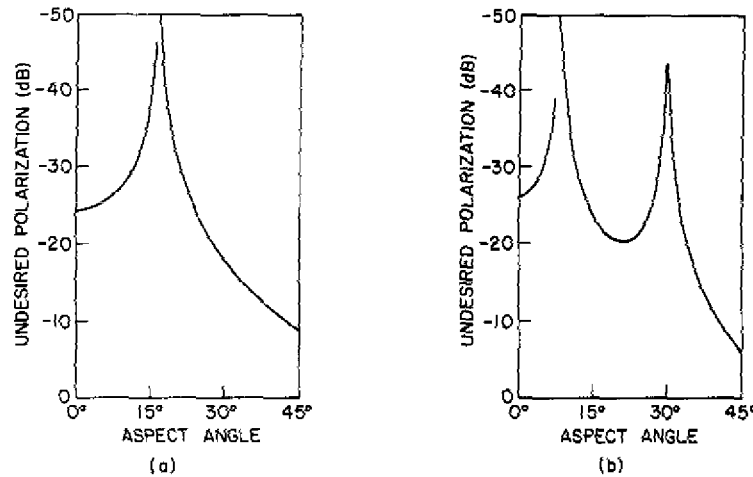


Fig. 7 — Performance vs aspect angle at (a) 3.0 GHz, and (b) 9.3 GHz

An initial design step for the lower frequency performance shaping is to move the ideal aspect as far from the mechanical axis (zero-aspect angle) as possible while retaining a sufficiently low value of the undesired polarization energy at zero aspect.

The significance of the zero-aspect performance is that all the undesired polarization energy reflects back into the feed appearing as a mismatch. Therefore, by specifying a maximum voltage standing-wave ratio (VSWR) of 1.2, for example, the corresponding allowable reflected energy may be calculated. For the VSWR of 1.2 max, the reflected energy must be -20.8 dB or less.

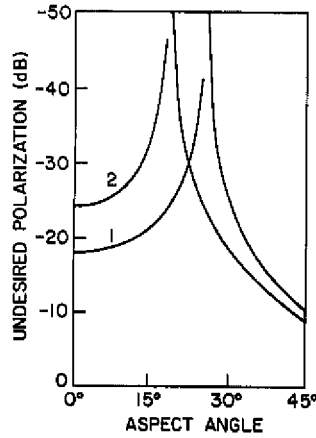
Typically, performance becomes worse at wide aspect angles as observed in Fig. 7. It is difficult to determine a specific lower performance limit at the wide aspect angles. At aspects other than near zero, the undesired energy does not reflect back into the feed so that a simple VSWR specification cannot be used. Also, at the wider aspect angles, less of the energy reflected from the mirror passes through the paraboloid. For example, at 45° aspect, none of the energy reflected from the mirror passes through the paraboloid so that the resultant energy transfer by the antenna is unaffected by the undesired polarization component.

At wide aspect angles, where part of the energy flows through the paraboloid, the undesired polarization represents energy scattered by the paraboloid. This appears as partial blockage of the beam. This blockage loss is relatively small, but it is asymmetrical and will have some effect on sidelobes and monopulse boresight.

In general, the capability of shaping the performance of the mirror is limited, particularly at the lower frequency. Figure 8 illustrates the observed consistent shape of the performance curve with con-

control of the trade-off of zero-aspect performance vs wide aspect angle performance. As zero-aspect performance decreases, wide aspect angle performance increases (curve 1 vs curve 2). Therefore, the basic approach is to adjust zero-aspect performance to approximately the minimum value necessary to meet the VSWR requirement thus allowing the best wide-angle performance.

Fig. 8 — Performance (curves 1 and 2) vs aspect angle at 3.0 GHz for two outer grid locations



The adjustment performed in Fig. 8 is achieved by changing the distance of the outer grid from the conducting surface ($\theta_1 + \theta_2$) which, in this case, is from 119° for curve 1 to 114.5° for curve 2. This adjustment also affects the performance at the higher frequency. However, it is observed that some parameters can be changed without significant change of the lower frequency performance, allowing relatively independent adjustment of higher frequency performance. For example, after the outer grid is located for desired lower frequency performance, the inner grid may be adjusted to regain the desired higher frequency performance without disturbing the lower frequency performance. This is illustrated in Fig. 9.

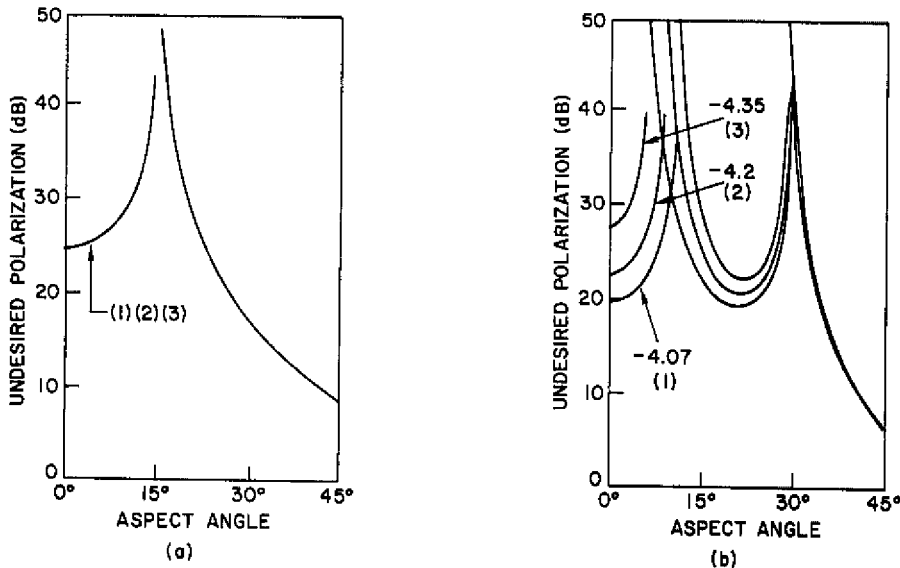


Fig. 9 — Performance (curves 1, 2, and 3) vs aspect angle for different inner grid normalized susceptances at (a) 3.0 GHz, and (b) 9.3 GHz

One problem in fabrication of the final wire grid twist reflector (see section on mirror fabrication) is that it is difficult to hold tolerances with the thickness of the outside epoxy/fiberglass protective surface. The variation of possible thickness resulted in a relatively wide range of capacitive susceptance values at the outer grid.

By experimenting with the effect of parameters on computed performance plots, it was found that reducing electrical separation between grids and the grid-to-conducting plane provides good results with high tolerance to variation in capacitive susceptance of the epoxy/fiberglass protective surface. Figure 10 illustrates the results of reducing electrical spacings to 28° for the conducting surface to inner grid, and 111° for the conducting surface to outer grid. The curves are plotted for outer grid normalized susceptance values ranging from 0.8 to 1.3 to demonstrate the high tolerance to variation of outer skin thickness.

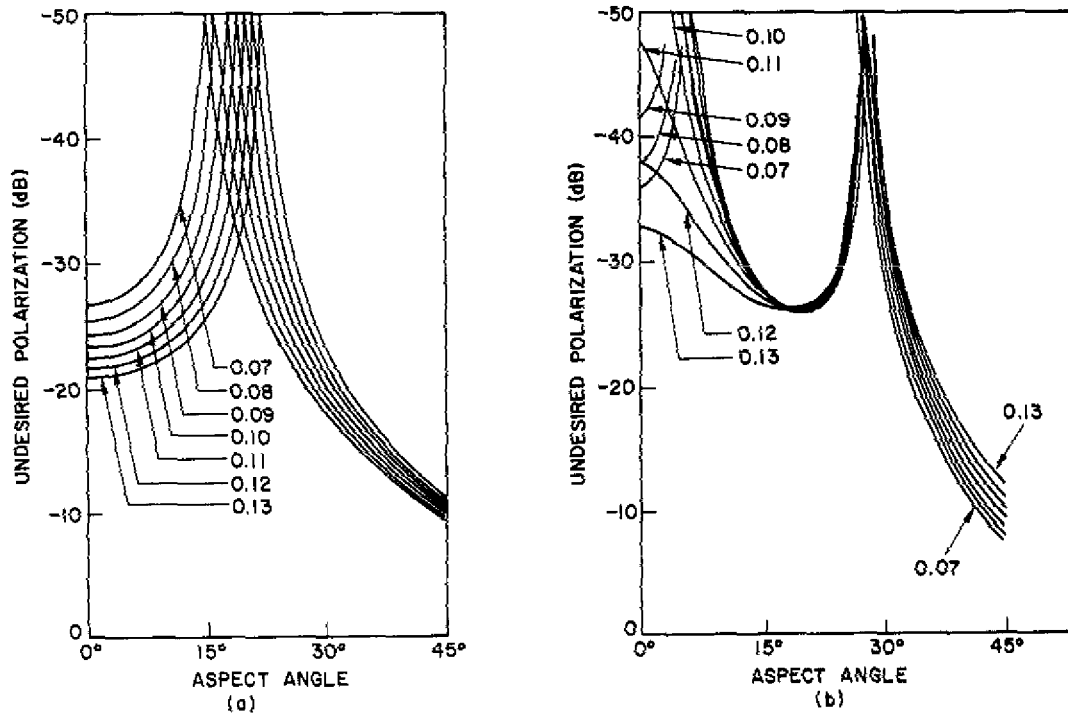


Fig. 10 — Twist reflector performance vs aspect angle for different normalized capacitive susceptance values at (a) 3.0 GHz, and (b) 9.3 GHz

Figure 7 also illustrates the trade-off considerations between zero-aspect performance and performance at other aspect angles. First, large aspect angle performance requires major parameter changes to alter its character; however, good performance need only be provided for aspect angles from zero to aspects where the signal no longer passes through the paraboloid. Therefore, the major trade-offs are between performance at zero aspect and at the 25° to 30° aspect. Similar to the lower frequency design, the best choice is to select the minimum performance at zero aspect which meets the VSWR requirement and provides the best performance in the 25° to 30° performance dip region.

A consideration of performance at wide aspect angles is that, as mentioned above, significant energy will pass to the side of the paraboloid where the undesired polarization energy will not be reflected by the paraboloid. This imperfectly rotated energy or undesired polarization energy is useful in the sense that the system is reciprocal, and echoes from the undesired polarization component will be received and contribute to echo energy. It is termed undesired because, if it is reflected by the paraboloid, it can be harmful to the transmitter or increase far-out sidelobes.

At very wide aspect angles, the undesired polarization completely misses the paraboloid and is of no consequence in terms of rf efficiency. The efficiency problem is a result of the shadowing of this polarization component at smaller aspect angles. Figure 11(b) plots the amount of blockage of the undesired polarization energy where 0 dB is 100% blockage. This curve assumes uniform illumination over the collimated beam. In practice, the blockage percentage will drop even more quickly vs aspect for a practical illumination taper. From an energy blockage standpoint, the cross-polarized energy plot of Fig. 7 should be modified to account for the fact that not all the energy is required to pass through the reflector (as illustrated in Fig. 11(a)). Figure 12 shows the results of including this effect. Thus, the actual energy lost because of the undesired polarization can be held to the order of -20 dB or less.

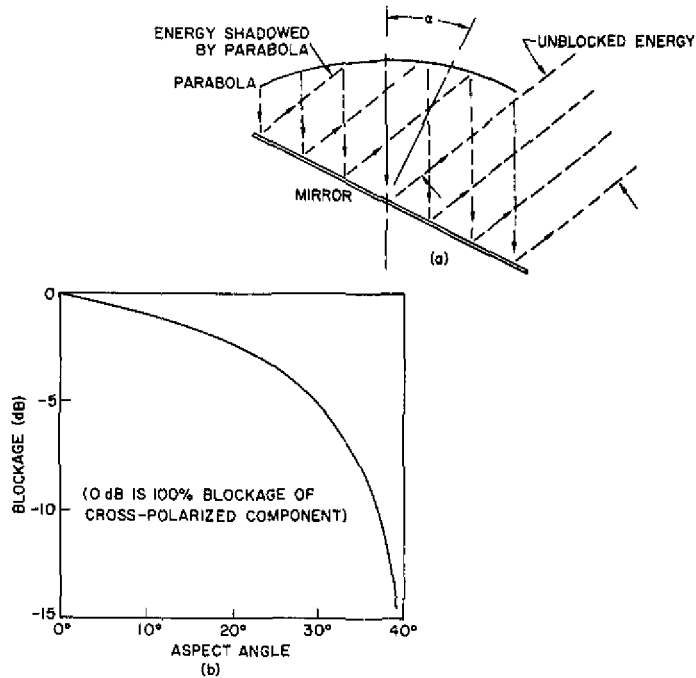


Fig. 11 — (a) Illustration, and (b) plot vs aspect angle of blockage of undesired polarization

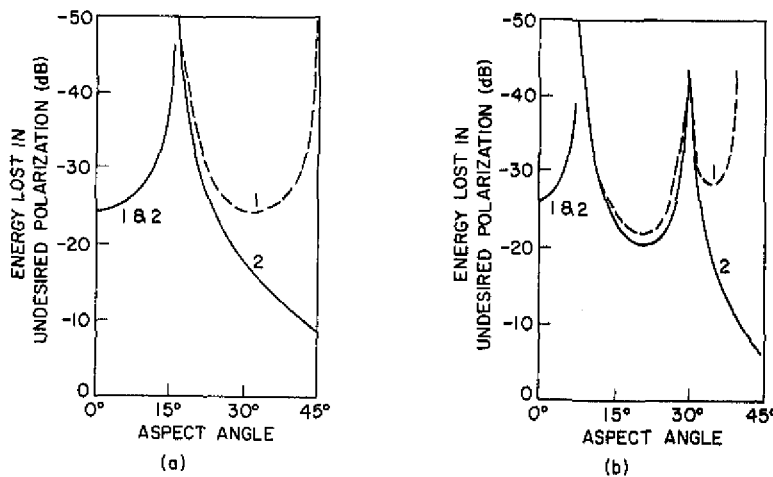


Fig. 12 — Energy lost vs aspect angle with (dashed curves—1) and without (solid curves—2) blockage consideration at (a) 3.0 GHz, and (b) 9.3 GHz

Other factors are significant, however, including the fact that the blockage is asymmetrical. This asymmetry can cause sidelobe levels to increase and potentially introduce a boresight shift. For values of -20 dB or lower, these asymmetry effects are not expected to be significant.

SPECIFIC PRACTICAL DESIGN TASKS

Three methods of mirror construction were studied. They are basically similar and the electrical differences concern the location and capacitive susceptance of dielectric structural support layers. The three methods are (a) wire grids for sample measurements with wires stretched between supports — this is the simplest configuration with no dielectric supporting the grids and no dielectric between grids; (b) grids etched on copper-clad dielectric with the dielectric skins holding the copper strips — this configuration is a dielectric outer layer with the etched copper grid on the inner surface, for both grids which are spaced by low dielectric, constant, low-loss, polyurethane foam layers; and (c) wire grids layed on the foam spacers and held with adhesive spray — this allows very small capacitive susceptance except for an outer layer of epoxy and thin fiberglass.

Samples of all three approaches were measured. The first configuration, although not practical for most mirror applications, gave good reference data on performance with no dielectrics involved. This configuration was limited by edge effects which were significant because of the wire support structure and because measured samples were relatively small.

A sample of the second configuration with etched strips was compared with a sample of the third configuration with wires. Although the performance vs aspect was similar, a small loss of about 1 dB or less was indicated with the measurements of the etched grid. No specific explanation was found; however, the adequacy of the copper thickness of the etched grids (0.0007 in. with 1/2 oz. copper) caused some concern. Although skin depth at S-band is only a small part of this thickness, the thin grid could potentially be a contributor to a small loss. Also, the etched grid width of only a few thousandths of an inch was difficult to produce and some small gaps in grid strips were observed.

Samples were tested in an anechoic chamber by using a variable polarization horn source and a movable receiving horn, as illustrated in Fig. 13. The receive horn was placed at locations corresponding to various beam scan angles, 2α , which are twice the aspect angles. A flat plate equal in size and shape to the twist reflector was used as a reference.

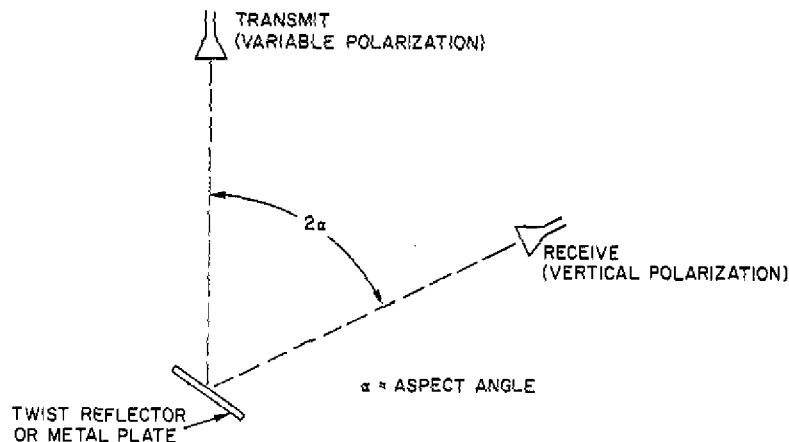


Fig. 13 — Setup for experimental sample measurements

Figure 14 shows typical data for three values of 2α . The reference plate was oriented to give a peak output at the receiver. Also, the transmitter and receiver polarization were parallel for peak reception. The transmitter polarization was rotated, causing the vertical line plot to go from peak output to noise. A short horizontal line was plotted where the antenna polarizations were parallel and at 90° .

This process was repeated with several twist reflector samples, but the peak response always occurred when the polarization twist equalled 90° as desired. The undesired component level, when the antenna polarizations were parallel, is indicated by the short horizontal line plot at the bottom of vertical plot. In some cases, the minimum coupling between antennas was a few decibels lower than the value measured when the two antennas were aligned for parallel polarization. This indicates that the maximum cross-polarized condition occurs at an antenna polarization slightly different than 90° .

The data in Fig. 14 show the comparison of the etched (printed) grid and wire grid twist reflectors with a flat metal plate as a reference. The following undesired polarization values illustrate readings from the data:

- $(2\alpha) = 10^\circ$: printed grid, -18 dB; wire grid, -32 dB
- $(2\alpha) = 20^\circ$: printed grid, -20 dB; wire grid, -34 dB
- $(2\alpha) = 30^\circ$: printed grid, -33 dB; wire grid, -22 dB

A major limitation of the experimental measurements was the edge effect of small samples. The wire grid used threaded rods on the edge for spacing the wires, and the etched grid terminated in open wires. Consequently, the results are qualitative but peak values of the line plots differ about 1 dB or less from the flat plate reference.

Figure 15 shows the calculated performance of a twist reflector mirror sample design compared with measured results. Considering the potential error from edge effect, which becomes increasingly worse with increasing aspect angle, there is a good qualitative match between measurement and theory.

TWIST REFLECTOR FINAL DESIGN

The specific values selected for this mirror antenna with wire grid construction, as shown in Fig. 15(a), provide a very good theoretical performance. The normalized grid susceptance values for the outer grid at S-band are $B_1/Y_0 = -2.277$ and $B_2/Y_0 = -4.216$. For convenient wire spacing and wire size that matches an available wire gauge, the calculated values are $B_1/Y_0 = -2.276$ and $B_2/Y_0 = -4.213$, giving the performance described in Fig. 15(b). The grid locations for this performance are 29.5° for the inner grid and 85° for the outer grid to inner grid spacing.

Although No. 39 wire was originally planned for the outer grid, it was found to be too delicate and was difficult to handle. Wire size No. 36 was used and compensated by increasing wire spacing to maintain the desired susceptance. Also, it was conveniently the same size wire as the inner grid. Since the larger wire spacing was approaching the limit indicated by Hannan [2], where grating lobes may result in energy scatter, samples were measured but no grating lobe problems were observed.

Two problems occurred in the fabrication process. The delivered precision cut dielectric core was thinner and apparently had a lower dielectric constant than specified. Also, the resultant dielectric skin was thicker than planned. The skin was made of 7 mil fiberglass and epoxy with the intent of maintaining approximately 7 mil finished thickness as accomplished with samples. However, more epoxy was applied than anticipated.

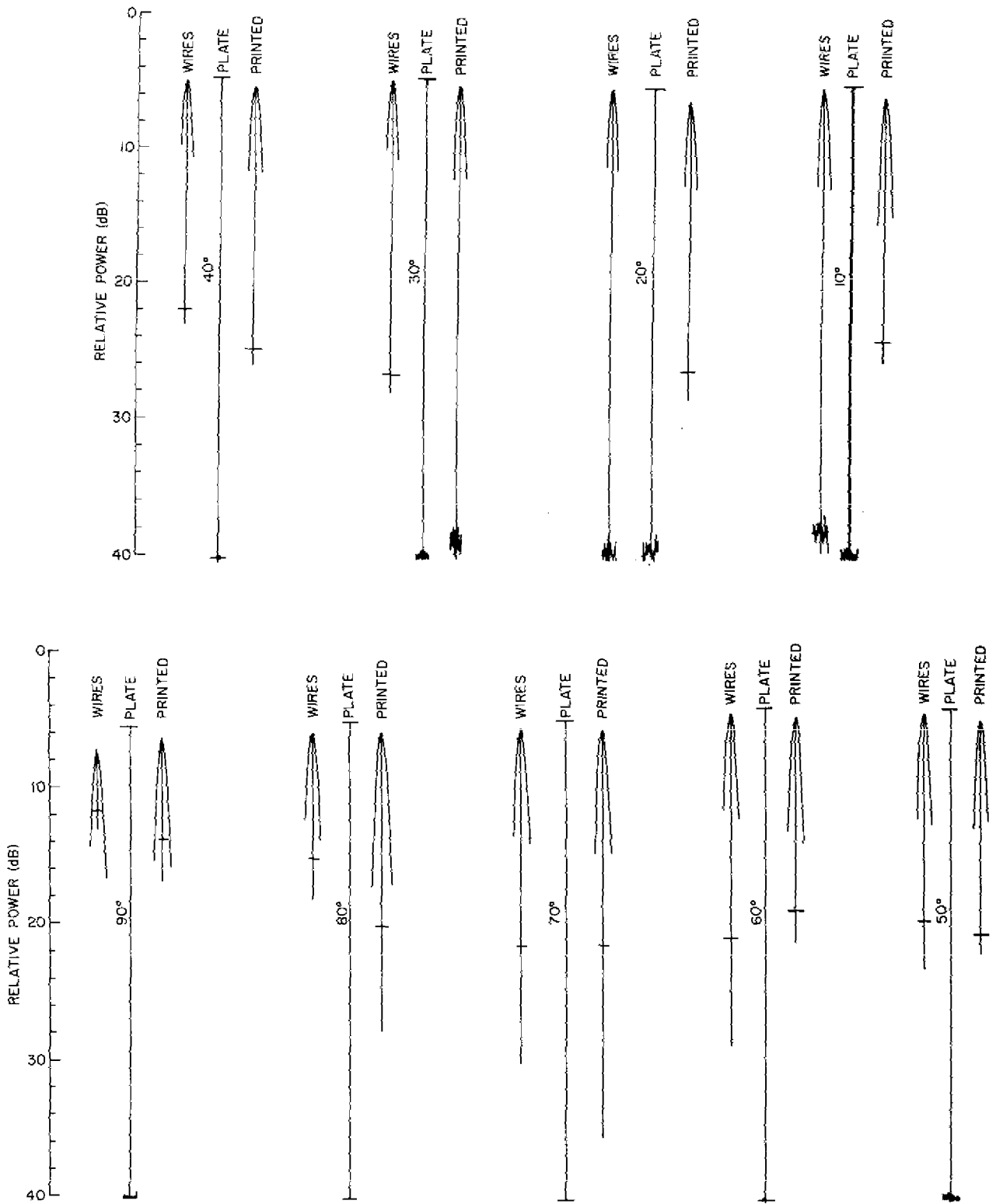


Fig. 14 — Data from measurements of 16-in. square twist reflector samples in anechoic chamber (indicated angle is twice the aspect angle)

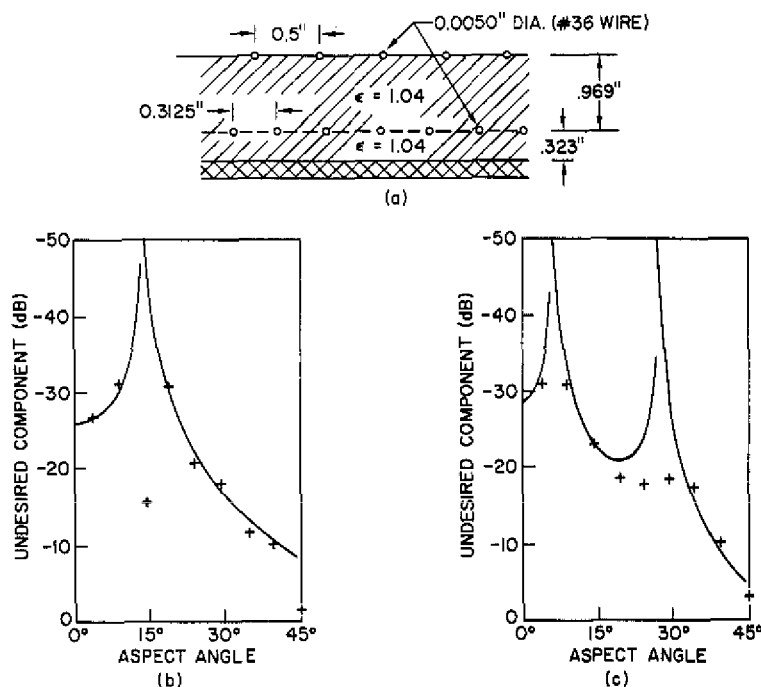


Fig. 15 — Twist reflector design (a), and comparison of theoretical data and sample measurements at (b) 3.0 GHz, and (c) 9.3 GHz

Fortunately, these two changes in parameters compensated each other in performance. The delivered core was estimated to give effective inner grid spacing from the conducting plane reduced to 28° as well as separation between grids reduced to 83° . The dielectric skin was estimated to give a normalized capacitive susceptance between 0.02 and 0.06. The performance for the new core thickness and this range of susceptance values is plotted in Fig. 16. The results show that very good performance is retained over this range of capacitive susceptance values.

MIRROR FABRICATION

As previously discussed, the wire construction was selected, since it provided the most consistent grid diameter and least potential for losses. The fabrication, by manually placing wires, seemed somewhat tedious, but was accomplished with only a few hours' effort.

The construction was a sandwich of lightweight, low-loss, and low-dielectric constant polyurethane foam and wire grids glued to an aluminum honeycomb base which provided the conducting surface. A spray adhesive (3M No. 90) was used. The first layer of foam was glued to the honeycomb base. The first wire grid was placed on the first layer of foam with a special jig for wire spacing and held in place with the spray adhesive. Figure 17 shows the wire-holding jig specially machined for precision spacing of the wires. Observe the layered edge of the twist reflector from the first darker layer, which is the aluminum honeycomb base (providing the conducting surface), to the first layer of foam (thinner layer), next the inner grid (not visible), then the outer layer of foam, and finally the outer grid wires in place ready for gluing. Figure 18 shows the wires being placed in position, and Fig. 19 shows the adhesive being sprayed on the outer grid. The grid wires were then trimmed at the edge of the twist reflector.

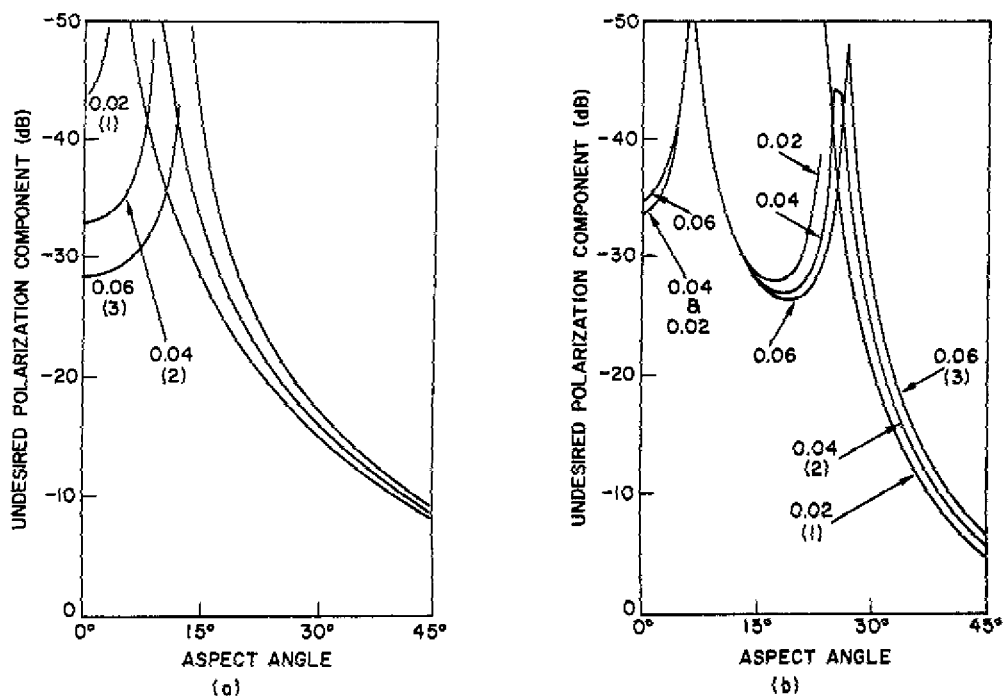


Fig. 16 — Twist reflector performance (curves 1, 2, and 3) for the indicated values of normalized capacitive susceptance of the outer protective layer at (a) 3.0 GHz, and (b) 9.3 GHz

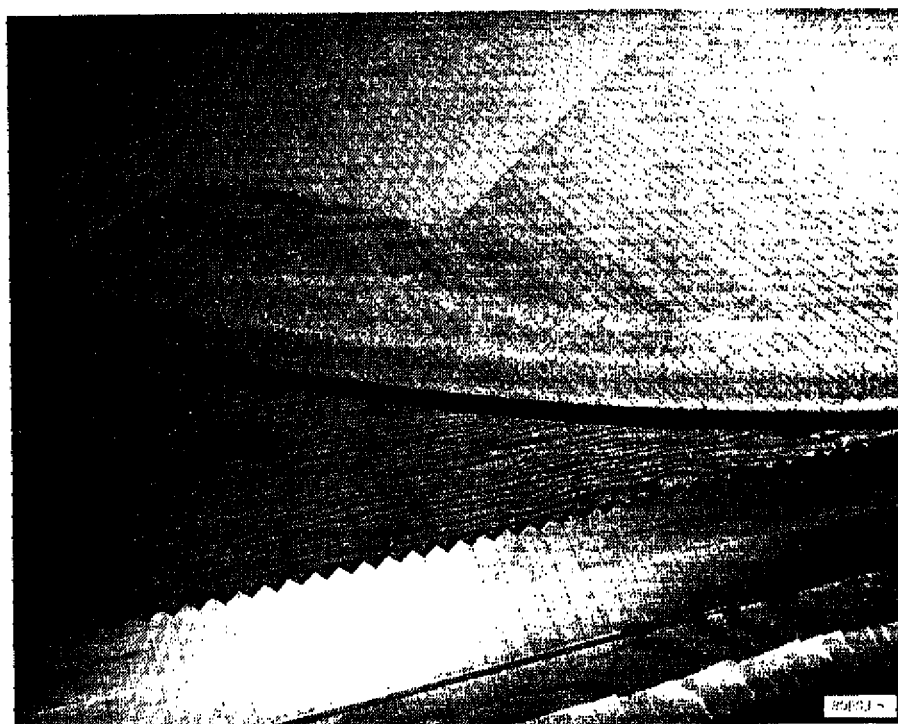


Fig. 17 — Partly contracted twist reflector and wire-spacing jig



Fig. 18 — Placing wires on twist reflector for outer grid



Fig. 19 — Spraying adhesive to hold outer grid wires in place

The twist reflector was then coated with 7 mil fiberglass impregnated with epoxy to provide a protective outer layer. The dual-band mirror with 2.18-m diameter and aluminum honeycomb base weighed 20 kg. This was within bounds for the necessary lightweight construction.

SUMMARY

A dual-band polarization twist mirror was constructed to operate at 3.0 and 9.3 GHz. Theory provided design parameters to obtain a perfect 90° polarization twist with a two-layer grid at one aspect angle. At other aspect angles, the polarization twist was not a perfect 90° , but its performance could be held to acceptable values.

A computer was programmed to plot twist reflector performance vs aspect angle. This allowed optimization of parameters to best fit practical fabrication and operational constraints. The mirror design and fabrication are described.

ACKNOWLEDGMENTS

The authors acknowledge Mr. Bernard Lewis for helpful guidance in the mirror antenna design and Dr. Robert Adams for assistance with the transmission line analysis. Mr. Billy Wright and Mr. Paris Coleman prepared test models using novel techniques that greatly simplified their fabrication while holding close tolerances. Also, Mr. James Titus provided valuable consultation and assistance with the fabrication process.

REFERENCES

1. P.T. Klass, "Special Series: Israeli Avionics—2," *Aviation Week Space Technol.* **108**(16), 38-50 (17 Apr. 1978).
2. P.W. Hannan, "Design for a Twistreflector Having Wideband and Wide-Angle Performance," ASTIA Document AD 306000, 1955.
3. B.L. Lewis and J.P. Shelton, "Mirror Scan Antenna Technology," *IEEE International Radar Conference Record*, Apr. 1980, pp. 279-283.
4. B.L. Lewis, "360° Azimuth Scanning Antenna Without Rotating RF Joints," U.S. Patent No. 3,916,416, 1975.
5. L.G. Josefsson, "A Broad-Band Twist Reflector," *IEEE Trans. Antennas Propag.* **AP-19**, 552-554, July 1971.
6. J.R. Wait, "Reflection at Arbitrary Incidence from a Parallel Wire Grid," *Appl. Sci. Res.* **4B**, 393-400 (1954-55).

Appendix

PERFORMANCE VS PLANE OF ANGLE OF INCIDENCE

The performance of a polarization twist mirror vs aspect angle has been generally treated as if there were no relation between the plane in which the aspect is taken and the direction of the grid wires. Most analyses of the wire grids are based upon the assumption that the aspect angle is in a plane that is normal to the wire grid as shown in Fig. 6 for an aspect angle α . However, further analysis of grid susceptance vs an arbitrary angle of incidence was performed by Wait [6]. He shows that grid susceptance is the same function of aspect angle (where wire spacing is small compared to a wavelength, and the wires are metallic) whether the plane of the angle of incidence is either parallel or perpendicular to the wire.

This is expressed by:

$$\frac{B_w}{Y_0} = \frac{\lambda}{S \cos \alpha \cos \beta} \cdot \frac{1}{\ln \left(\frac{S}{\pi d} \right)} \quad (A1)$$

where α and β are defined in Fig. 6,

S is wire spacing between center, and

d is wire diameter.

Aspect angles in other planes are of interest, particularly the plane at 45° to the grid wires. In this case, B_w/Y_0 does not have a simple cosine relative to aspect angle.

Figure A1 illustrates the geometry of an aspect angle γ in a plane of orientation ω relative to the α aspect plane which is perpendicular to the grid wires (see Fig. 6). The relation of γ and ω to α and β can be observed, and the function $\cos \alpha \cos \beta$ of Eq. (A1) can be expressed in terms of γ and ω . It is observed in Fig. A1 that

$$\cos \alpha = \frac{\cos \gamma}{\sqrt{\cos^2 \gamma + \sin^2 \gamma \cos^2 \omega}} \quad (A2)$$

and

$$\cos \beta = \frac{\cos \gamma}{\sqrt{\cos^2 \gamma + \sin^2 \gamma \sin^2 \omega}} \quad (A3)$$

Therefore,

$$\cos \alpha \cos \beta = \frac{\cos^2 \gamma}{\sqrt{\cos^2 \gamma + \sin^2 \gamma \cos^2 \omega} \sqrt{\cos^2 \gamma + \sin^2 \gamma \sin^2 \omega}} \quad (A4)$$

The plane of major interest is where $\omega = 45^\circ$ and Eq. (A4) reduces to

$$\cos \alpha \cos \beta = \frac{2 \cos^2 \gamma}{1 + \cos^2 \gamma} \quad (A5)$$

The aspect angle function vs aspect is plotted in Fig. A2 for the case where $\omega = 0^\circ$ or $(\cos \alpha)$ and $\omega = 45^\circ$ $2 \cos^2 \gamma / (1 + \cos^2 \gamma)$. It is observed that there is very little difference in the aspect angle function as the plane of the aspect angle is rotated for the aspect angle range of interest (0° to 45°).

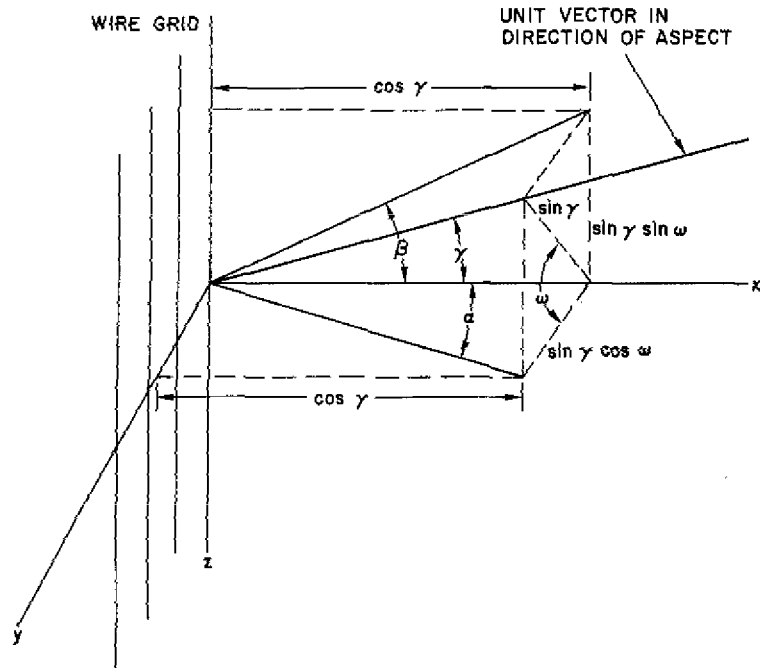


Fig. A1 — Parameters for illustration of variable aspect geometry

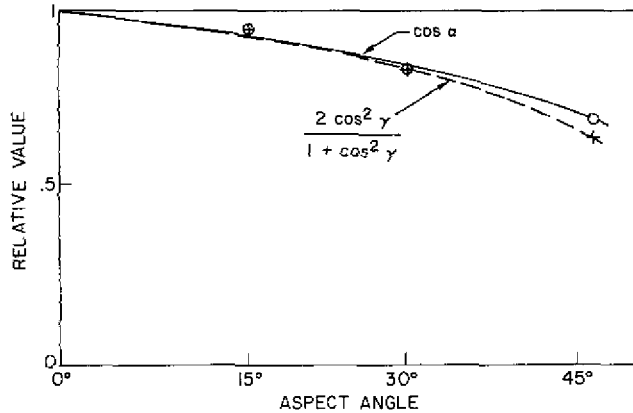


Fig. A2 — Variation vs aspect angle for a 0° ($\cos \alpha$) and a 45° [$2 \cos^2 \alpha / (1 + \cos^2 \alpha)$] orientation relative to the grid wires

Plots of the undesired polarization component $P(u)$, (see Eq. 17), are used in the report to assess mirror performance. Because of the different function B_w vs aspect angle, the possibility of a significant difference in performance between the parallel or perpendicular aspect plane and the 45° aspect plane was a concern. Figure A3 was plotted for the parallel and perpendicular planes and the 45° plane. Insignificant differences were observed.

All plots used in this report were checked for parallel, perpendicular, and 45° aspect planes, and no significant differences were observed. Therefore, it is concluded that the performance is essentially independent of the angle of the plane in which the angle of incidence occurs.

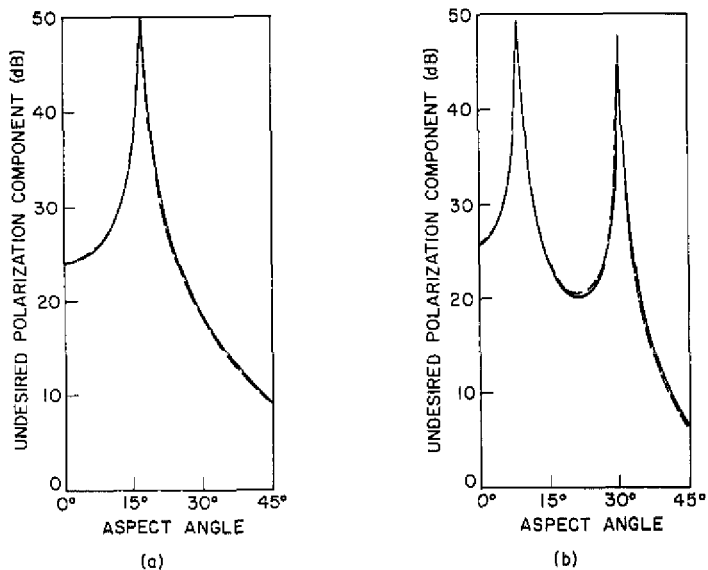


Fig. A3 -- Undesired polarization, parallel or perpendicular to the grid (dashed line) and at 45° to the grid (solid line) at (a) 3.0 GHz, and (b) 9.3 GHz